NANO LETTERS

pubs.acs.org/NanoLett Letter

Sugar-Nanocapsules Imprinted with Microbial Molecular Patterns for mRNA Vaccination

Sejin Son, Jutaek Nam, Ilia Zenkov, Lukasz J. Ochyl, Yao Xu, Lindsay Scheetz, Jinjun Shi, Omid C. Farokhzad,* and James J. Moon*

Cite This: *Nano Lett.* 2020, 20, 1499−1509 Read Online

ACCESS | Metrics & More | Article Recommendations | Supporting Information

ABSTRACT: Innate immune cells recognize and respond to pathogen-associated molecular patterns. In particular, polysaccharides found in the microbial cell wall are potent activators of dendritic cells (DCs). Here, we report a new class of nanocapsules, termed sugar-capsules, entirely composed of polysaccharides derived from the microbial cell wall. We show that sugar-capsules with a flexible polysaccharide shell and a hollow core efficiently drain to lymph nodes and activate DCs. In particular, sugar-capsules composed of mannan (Mann-capsule) carrying mRNA (mRNA) promote strong DC activation, mRNA translation, and antigen presentation on DCs. Mann-capsules elicit robust antigen-specific CD4+ and CD8α+ T-cell responses with antitumor efficacy *in vivo*. The strategy presented in this study is generally applicable for utilizing pathogen-derived molecular patterns for vaccines and immunotherapies.

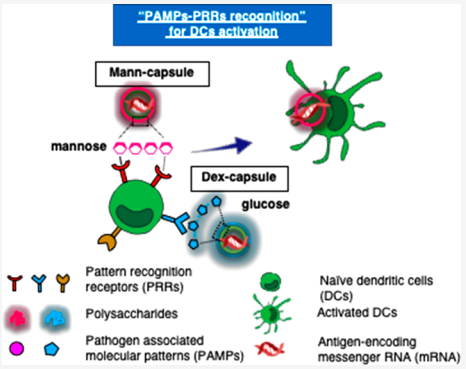

KEYWORDS: *nanoparticle, polysaccharide, mRNA, dendritic cell, vaccine*

Dendritic cells (DCs) are professional antigen-presenting cells (APCs) that phagocytose, process, and present antigens to T-cells in lymph nodes (LNs) to initiate antigen-specific immune responses.[1] DCs recognize conserved microbial molecular structures of pathogens, termed pathogen-associated molecular patterns (PAMPs), via the engagement of pattern recognition receptors (PRRs).[2] Recognition of PAMP−PRR, as the first line of the host defense mechanism, triggers the secretion of inflammatory cytokines from DCs and coordinates the induction of adaptive immune responses against pathogens.[3] Therefore, integrating the PAMP−PRR interactions into biomaterials may allow for efficient engagement of innate immune cells and induction of adaptive immune responses.

There has been extensive effort to develop therapeutic cancer vaccines based on peptides and proteins to induce cytotoxic T-cell lymphocytes (CTLs) against cancer cells.[4,5] Compared with conventional subunit vaccines, mRNA-based vaccines offer distinct advantages:[6,7] (1) they have excellent safety profiles without the risk of insertional mutagenesis; (2) transient intracellular mRNA expression allows repeated boost vaccinations; (3) they are not restricted to patients' human leukocyte antigen (HLA) subtype; (4) they can be designed to encode multiple epitopes as well as immunostimulatory domain or danger signals in a single mRNA molecule, and (5) their GMP manufacturing process is well established. Despite these advantages, inherent biological instability and poor pharmacokinetics of mRNA have long been major obstacles.[7,8] Various mRNA delivery strategies have been developed in the past with varying degrees of success, including intranodal delivery of naked mRNA,[9] protamine-based,[10,11] cationic liposomal,[12−14] and polymeric[14,15] mRNA delivery formulations; however, it remains challenging to achieve selective delivery of mRNA to APCs in lymphoid organs and elicit robust CTL responses with potent antitumor efficacy.

Microbial cell walls have distinct polysaccharides with repeating carbohydrate units that are recognized by PRRs on DCs, leading to potent immune stimulation.[16,17] Various polysaccharides have been investigated so far, including mannan,[18−20] glucan,[21] and their derivatives[22] for the purpose of immune regulation, interactions with DCs,[18] and vaccine applications.[23] For example, mannan (polysacharides found in the cell wall of yeasts) and dextran (a complex branched glucagon from bacteria) are reported to interact with various PRRs, including C-type lectins (e.g., Dectin and Mincle), toll-like receptors (TLRs), CD206 (lectin-like mannose receptor), and CD209 (DC-SIGN, dendritic cell-specific intercellular adhesion molecule 3-grabbing nonintegrin) expressed on innate immune cells, including DCs, monocytes, and macrophages.[24−26] While the exact mechanisms of action remain

Received: August 23, 2019
Revised: February 1, 2020
Published: February 5, 2020

https://dx.doi.org/10.1021/acs.nanolett.9b03483
Nano Lett. 2020, 20, 1499−1509

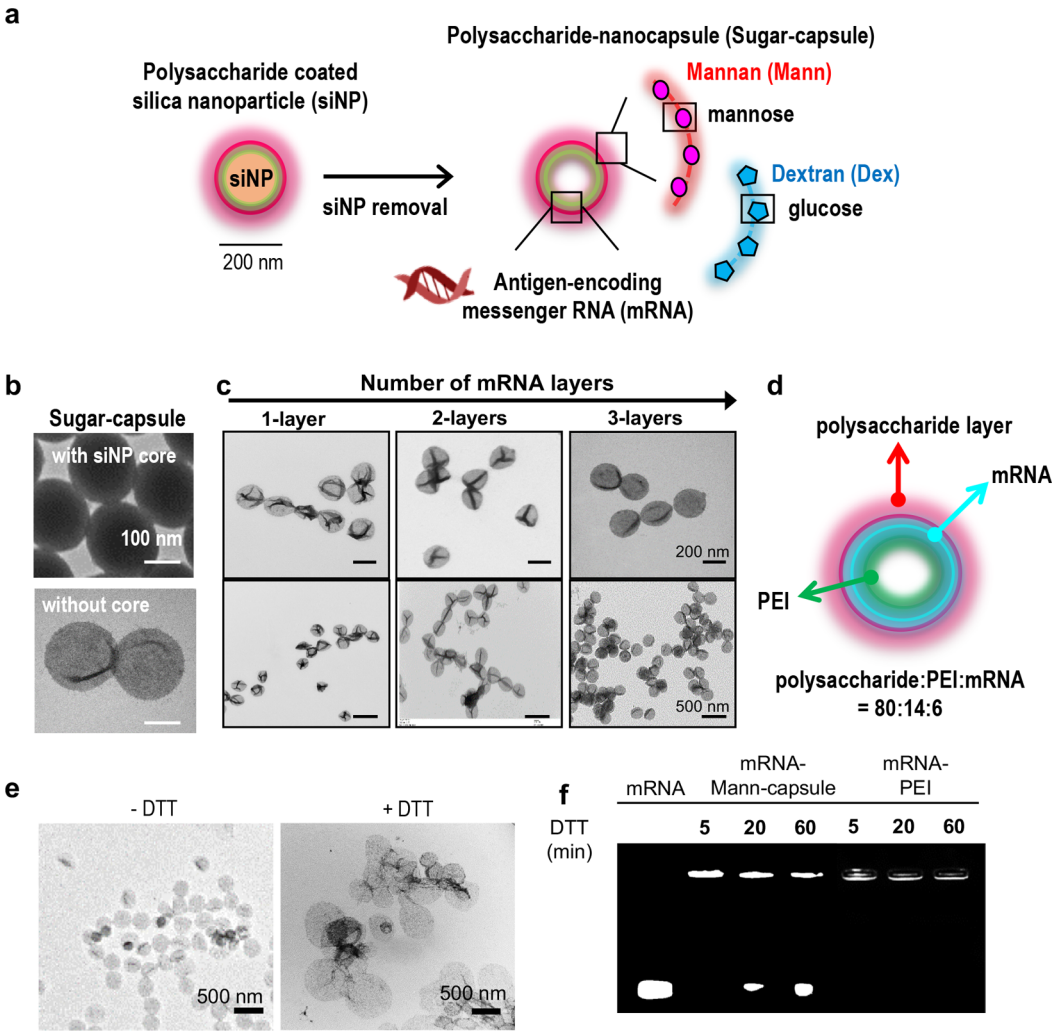

Figure 1. (a) Schematic illustration of synthesis of mRNA-loaded sugar-capsules. (b) TEM images of sugar-capsules before (top) and after (bottom) removal of a core silica nanoparticle. (c) TEM images of sugar-capsules with multilayered mRNA loading at high (top) and low (bottom) magnification. (d) Illustration of an mRNA-sugar-capsules with the weight ratio of components. (e, f) Evaluation of redox-responsive degradability of sugar-capsules. (e) TEM images of Mann-capsules and (f) agarose gel image of mRNA-Mann-capsules or mRNA-PEI after DTT treatment.

unclear, recent studies have suggested that structural and chemical compositions of polysaccharides found on a pathogen's surface dictate the specificity and extent of immune activation.[17] Here, we have developed nanocapsules entirely composed of microbial polysaccharides mimicking the structural and immunological properties of the microbial cell wall (Figure 1a). Our synthetic sugar-capsules composed of a mannan or dextran polysaccharide shell with a hollow core serve as a novel nanosystem for engaging DCs, and here we demonstrate their immunogenicity and utility as a platform for mRNA vaccine delivery applications.

We constructed sugar-capsules on carboxylated silica nanoparticles (siNPs, ~200 nm in diameter) employed as a sacrificial template. Specifically, siNPs were first coated with polyethylenimine (PEI, 25 kDa) that served as a backbone for sugar-capsules. PEI was cross-linked using a reduction-sensitive cross-linker, dimethyl 3,3′-dithiobispropionimidate·2HCl (DTBP), which rendered the nanocapsules with structural robustness and intracellular degradability. Simple incubation of PEI-siNP with mRNA led to efficient loading of mRNA. The resulting mRNA-loaded PEI-siNPs were incubated with polysaccharide-CHO to coat the external layer with polysaccharides. In particular, we constructed two classes of PAMP-imprinted sugar-capsules using either mannan (Mann-capsule) or dextran (Dex-capsule). After confirming the amine−aldehyde reaction between PEI and polysaccharide-CHO by quantification of the remaining polysaccharide-CHO in solution (49 ± 8.2% reaction yield), we removed the siNP core by incubation with ammonium fluoride for 5 min at room temperature (RT). The resulting hollow-core sugar-capsules appeared as collapsed nanostructures under TEM (Figure 1b). Compared with the 200 ± 3 nm diameter of template siNP, the hydrodynamic size of sugar-capsules slightly increased to 226 ± 13 nm, and the surface charge of the template siNPs was converted from −30 ± 1 to 60 ± 1 mV after PEI coating and finally to −1 ± 1 and −10 ± 1 mV after coating with dextran or mannan, respectively (Supporting Figure S1a,b). There was no significant change in the hydrodynamic size of formulation at each step (Supporting Figure S1a). PEI cross-linking with DTBP did not affect the surface charge of PEI-siNP at 63 ± 0.02 mV, and mRNA coating reduced the surface charge to 32 ± 0.5 mV (Supporting Figure S1b). As mRNA was deposited by 1−3 cycles of layer-by-layer (LbL) coating with mRNA and PEI, we observed highly efficient mRNA loading (~100%) for

https://dx.doi.org/10.1021/acs.nanolett.9b03483
Nano Lett. 2020, 20, 1499−1509

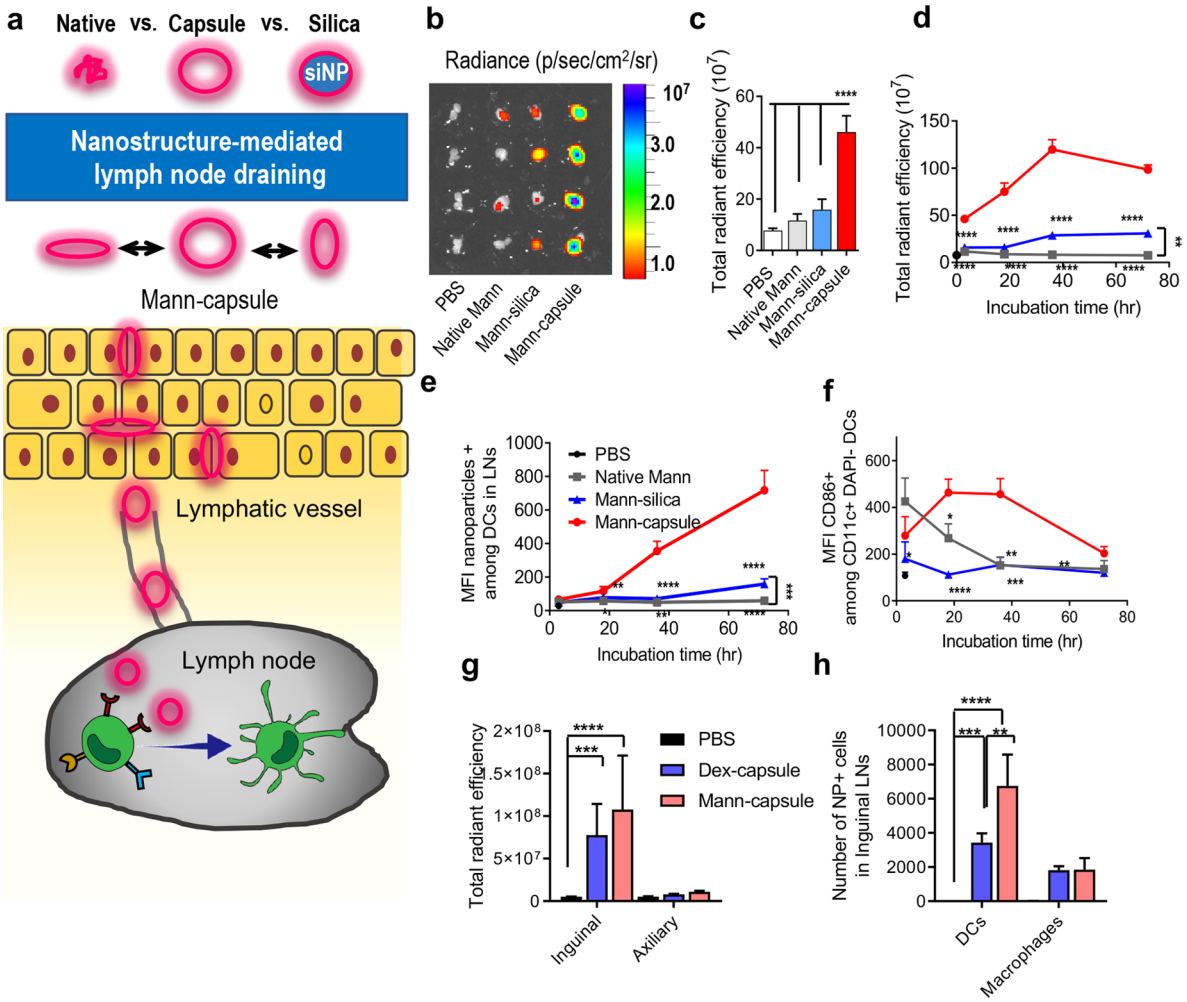

Figure 2. (a) Sugar-capsules with a hollow core efficiently drain to LNs after subcutaneous administration. (b–f) C57BL/6 mice were administered s.c. with Mann-Cy5.5 formulated as native Mann, Mann-silica, or Mann-capsules. (b) Draining inguinal LNs were imaged and quantified for Cy5.5 signal by IVIS at (c) 3 h postinjection or (d) over time at 3, 18, 36, and 72 h post injections. Mean fluorescence intensity (MFI) of (e) Mann-Cy5.5+ cells and (f) MFI of CD86 signal among CD11c+ DCs in inguinal LNs was measured over time by flow cytometric analysis. (g, h) C57BL/6 mice were administered s.c. with either Dex-capsules or Mann-capsules tagged with Cy5.5 and assessed for (g) the total radiant efficiency of Cy5.5 signal in the excised inguinal and axillary LNs by IVIS and (h) the number of capsule+ DCs and macrophages within inguinal LNs at 15 h postinjection. The data show means ± s.e.m. Statistical significance was calculated by (c,g,h) one-way ANOVA or (d–f) two-way ANOVA, followed by the Bonferroni multiple comparisons post-test. $^{*}P < 0.05$, $^{**}P < 0.01$, $^{***}P < 0.001$, and $^{****}P < 0.0001$.

each layer of coating, and mRNA remained intact after removal of the silica-NP core by etching with ammonium fluoride (Supporting Figures S2 and S3). The resulting sugar-capsules maintained their undeformed spherical shape, as shown by the TEM images, and sugar-capsules exhibited colloidal stability in high serum as well as after freeze–thawing conditions (Figure 1c and Supporting Figure S4), suggesting that LbL deposition of mRNA rendered the capsules rigid and stable. The final sugar-capsule formulations were composed of polysaccharide:PEI:mRNA = 80:14:6 by weight ratio, as determined by GPC analysis and TNBSA assay (Supporting Figure S5 and Figure 1d). Upon treatment with DTT, sugar-capsules were disrupted to debris, as shown by TEM images (Figure 1e), suggesting reduction-sensitive degradation of sugar-capsules. In addition, we confirmed efficient mRNA release from sugar-capsules in response to DTT treatment (Figure 1f). In contrast, the mRNA/PEI complex did not exhibit DTT-responsive mRNA release.

Efficient lymphatic drainage is a crucial step for vaccine delivery and elicitation of robust T-cell responses. While prior works have examined lymphatic delivery of nanoparticles based on their size,[27−29] surface charge,[30−32] and PEGylation,[31,33,34] it remains relatively unknown how the ridigity of nanoparticles affects their lymphatic drainage. Therefore, we examined whether sugar-capsules with their hollow, flexible nanostructures would improve lymphatic delivery and accumulation in LNs (Figure 2a). First, we prepared control NPs with similar physicochemical properties as sugar-capsules except for rigidity; bare silica NPs and Mann-coated siNPs (Mann-silica with a rigid silica template core) exhibited a similar hydrodynamic size and negative zeta potential as Mann-capsules (Supporting Figure S6). Whereas bare silica NPs and Mann-silica with an ∼220 nm diameter failed to pass through a 200 nm pore-sized membrane, ∼220 nm Mann-capsules readily passed through 200 nm as well as 100 nm pore membranes, and we even observed ∼30% recovery after extrusion through a 50 nm pore membrane (Supporting Figure S7), thus showing high deformability of Mann-capsules.

We conjugated Cy5.5 to Mann-capsules and confirmed their serum stability (Supporting Figure S8). When administered s.c.

https://dx.doi.org/10.1021/acs.nanolett.9b03483
Nano Lett. 2020, 20, 1499−1509

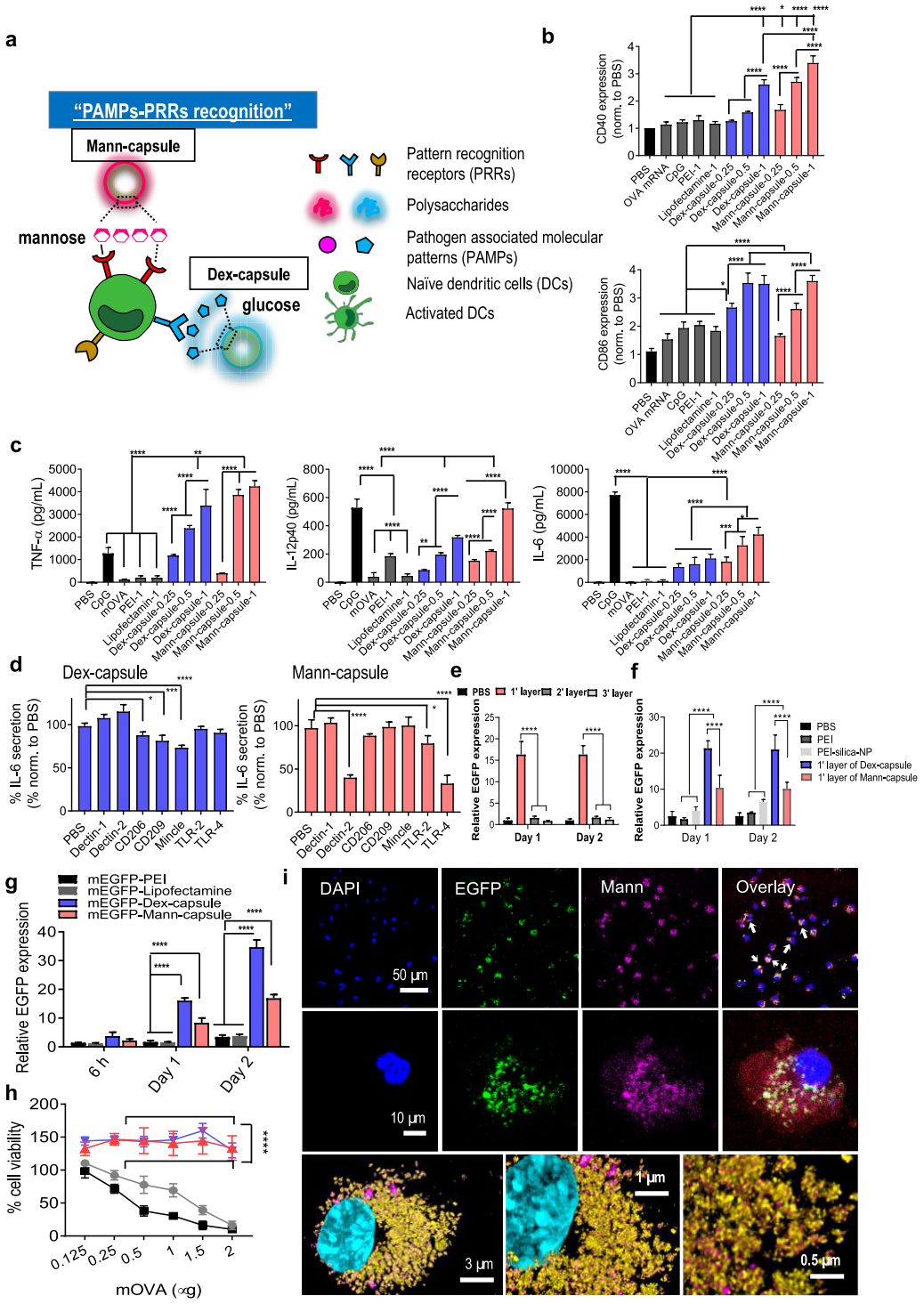

Figure 3. (a) Schematic illustration of the engagement and activation of DCs by Mann- or Dex-capsules. (b) Expression levels of CD40 (top) and CD86 (bottom) costimulatory signals and (c) secretion of pro-inflammatory TNF-α, IL-12p40, and IL-6 from BMDCs incubated with indicated formulations. (d) Secretion of IL-6 was measured after incubating sugar-capsules with BMDCs in the presence of blocking antibodies against various PRRs. (e–g) Evaluation of mRNA translation by quantifying EGFP signal after incubating BMDCs with various mEGFP formulations. We (e) varied the number of LbL layers for Dex-capsules and (f, g) compared Dex- and Mann-capsules to control groups. (i) Confocal microscopy images of BMDCs incubated with mEGFP-Mann-capsules. Nuclear DAPI (blue), EGFP (green), and Mann-Cy5.5-capsule (pink) are shown at various magnifications. (h) Cytotoxicity was measured after incubating BMDCs with a varying amount of mOVA-sugar-capsules. The data show means ± s.e.m. Statistical significance was calculated by (b–d) one-way ANOVA or (e, g) two-way ANOVA, followed by the Bonferroni multiple comparisons post-test. *P < 0.05, **P < 0.01, ***P < 0.001, and ****P < 0.0001.

at the tail base, Cy5.5-Mann-capsules efficiently drained to inguinal LNs, showing a significantly higher fluorescence signal at 3 h, compared with native Mann or Mann-silica (P < 0.0001, Figure 2b,c). A significantly elevated level of Mann-capsules was detected in inguinal LNs over 72 h after s.c. administration (Figure 2d). In particular, CD11c+ DCs in inguinal LNs

https://dx.doi.org/10.1021/acs.nanolett.9b03483
Nano Lett. 2020, 20, 1499–1509

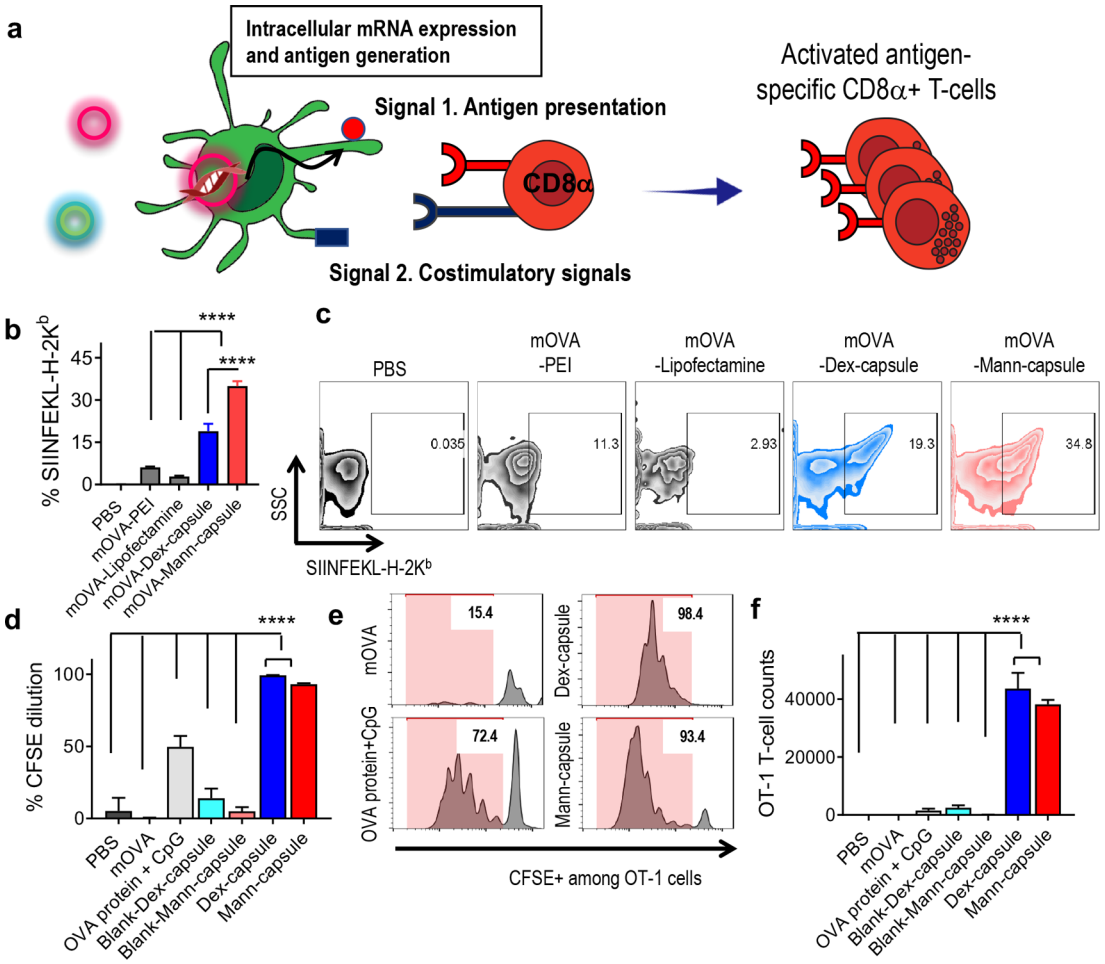

Figure 4. (a) Schematic illustration of antigen presentation and cross-priming of CD8a+ T-cells mediated by mRNA-loaded sugar-capsules. (b, c) BMDCs were incubated with mOVA formulated with either PEI, lipofectamin, Dex-capsules, or Mann-capsules, and (b) the frequency of DCs presenting SIINFEKL-H-2K^b complex with (c) the representative scatter plots are shown. (d–f) CFSE-labeled OT-I CD8α+ T-cells were cultured with BMDCs pulsed with various mOVA formulations, and (d) CFSE dilution, (e) the representative histograms, and (f) the number of expanded OT-1 CD8α+ T-cells were quantified by flow cytometric analyses. The data show means ± s.e.m. Statistical significance was calculated by one-way ANOVA, followed by the Bonferroni multiple comparisons post-test. ****$P < 0.0001$.

showed a strong Mann-capsule signal over 72 h (Figure 2e), and DCs exhibited an activated phenotype with increased expression of CD86 costimulatory ligand over 36 h *in vivo* (Figure 2f). In contrast, native Mann was rapidly cleared away with a minimal fluorescence signal in LNs, while Mann-silica showed a slight increase in Cy5.5 fluorescence in LNs over 72 h (Figure 2d–f) with minimal expression of CD86 on DCs (Figure 2f). Based on this, we speculate that efficient lymphatic trafficking of Mann-capsules is mediated by both passive transport of flexible nanocapsules and DC-mediated active transport, while Mann-silica with a rigid core mainly reaches LNs by active transport by peripheral DCs. In addition, we compared the lymphatic draining of Mann-capsules and Dex-capsules. After 15 h of s.c. administration, we observed a strong Cy5.5 fluorescence signal for both Dex- and Mann-capsules in inguinal LNs but not in axillary LNs (Figure 2g). Interestingly, quantification by flow cytometry revealed an increased association of Mann-capsules among DCs, compared with Dex-capsules (Figure 2h), potentially due to the presence of mannose receptors on DCs.[18,20] Correlating with these results, we also observed preferential uptake of Mann-capsules over Dex-capsules by bone-marrow-derived dendritic cells (BMDCs) *in vitro*, whereas similar uptake of Mann- and Dex-capsules was observed among bone-marrow-derived macrophages (BMDMs) (Supporting Figure S9).

Having shown efficient LN draining of sugar-capsules, we next investigated the immunological effects on DCs using sugar-capsules loaded with mRNA encoding a model antigen, ovalbumin (mOVA). For comparison, CpG, a potent Toll-like receptor 9 (TLR-9) agonist, was employed as a positive control.[35] In addition, we included PEI (cationic polymer)[36] and lipofectamine (cationic liposome) in our comparison, as these are widely used gene transfection agents. First, we examined the activation of BMDCs after incubation with sugar-capsules carrying mRNA. Mann- and Dex-capsules were efficiently taken up by BMDCs (Supporting Figure S10), triggering dose-dependent upregulation of CD40 and CD86 on BMDCs (Figure 3a,b). In contrast, BMDCs incubated with mRNA-PEI or mRNA-lipofectamine exhibited minimal upregulation of CD40 and CD86. Notably, Mann- and Dex-capsules also induced stronger expression of CD40 and CD86 on BMDCs, compared with CpG ($P < 0.0001$, Figure 3b). Mann- and Dex-capsules also promoted robust secretion of TNF-α, IL-12p40, and IL-6 from BMDCs (Figure 3c). These results show inherent immunostimulatory properties of Mann- and Dex-capsules without the use of any exogenous adjuvant

https://dx.doi.org/10.1021/acs.nanolett.9b03483
Nano Lett. 2020, 20, 1499–1509

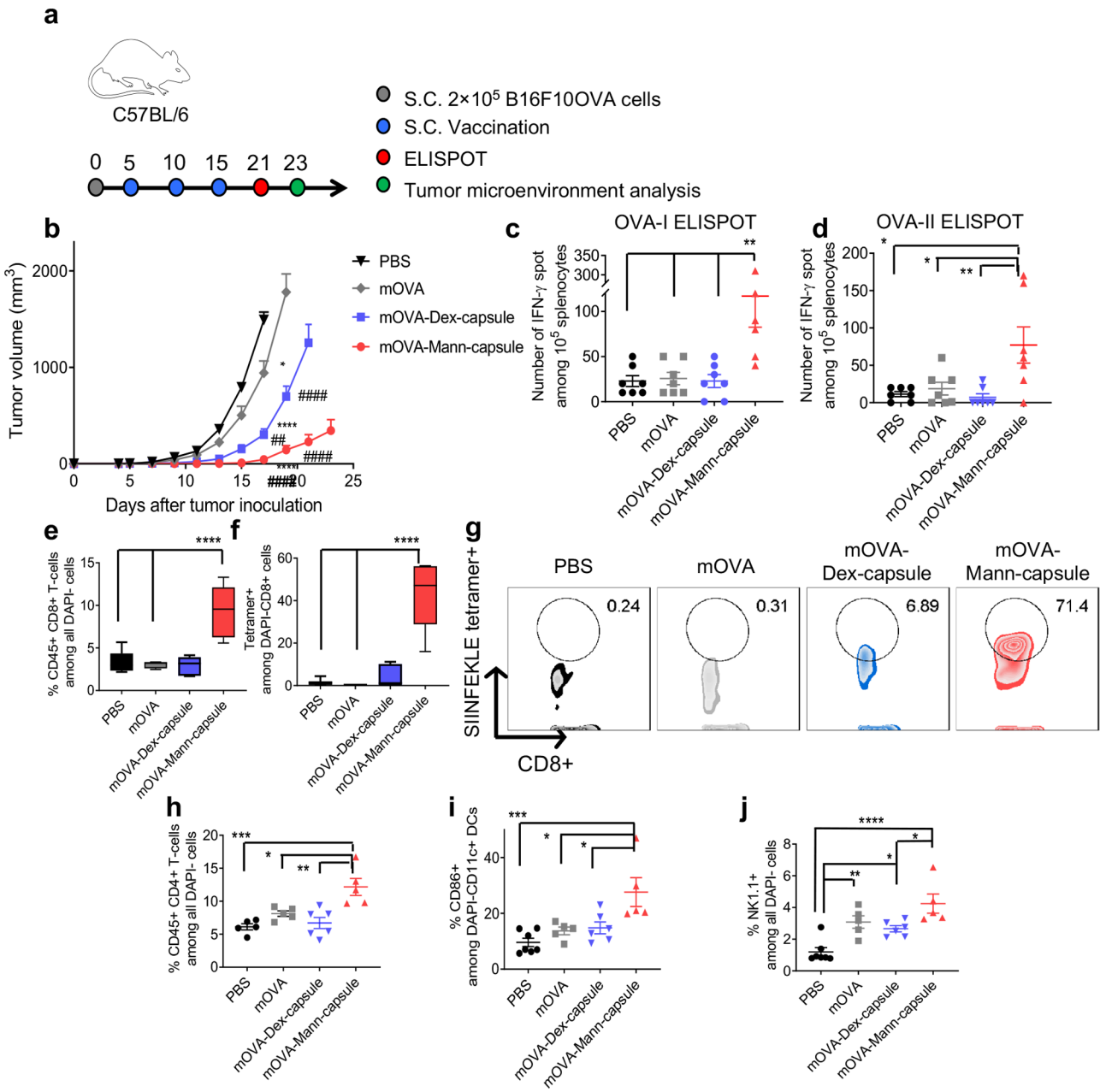

Figure 5. Antitumor efficacy of mOVA-loaded sugar-capsules. (a) C57BL/6 mice were inoculated with B16F10OVA cells at the right s.c. flank on day 0 and treated with the indicated formulations on days 5, 10, and 15. (b) Tumor growth was measured over time, and splenocytes were analyzed by ELISPOT on day 21 for (c) OVA-I-specific CD8α+ T-cells and (d) OVA-II-specific CD4 T-cells. (e–j) Tumors were analyzed by flow cytometry on day 23. Shown are the frequency of (e) CD8a+ T-cells, (f) OVA-specific CD8a+ T-cells, and (g) their representative scatter plots. Also, the frequency of (h) CD4+ T-cells, (i) CD86+CD11c+ DCs, and (j) NK1.1+ natural killer cells within the tumor microenvironment. The data show means ± s.e.m. Statistical significance was calculated by (b) two-way ANOVA or (c–j) one-way ANOVA, followed by the Bonferroni multiple comparisons post-test. *P < 0.05, **P < 0.01, ***P < 0.001, and ****P < 0.0001. * and # in part b indicate statistical differences compared with PBS and mOVA, respectively.

molecules. To delineate how Mann- and Dex-capsules activated BMDCs, we treated BMDCs with blocking antibodies against various PRRs, followed by incubation with sugar-capsules and quantification of IL-6 release. Mann-capsule-mediated secretion of IL-6 was significantly decreased in the presence of blocking antibodies against Dectin-2 or TLR-4 (P < 0.0001, Figure 3d), while Dex-capsule-mediated secretion of IL-6 was reduced in the presence of antibodies against CD206, CD209, or Mincle (P < 0.05, P < 0.001, and P < 0.0001, respectively, Figure 3d). Mann-capsules, but not Dex-capsules, activated HEK-blue TLR4 cells, but we did not observe activation of HEK-blue TLR9 cells with either Mann- or Dex-capsules (Supporting Figure S11). Taken all together, these results suggest that Mann- and Dex-capsules interact with distinct PRRs on DCs and serve as strong activators of DCs.

Next, we evaluated sugar-capsules as a platform for mRNA transfection. We examined the translation of mRNA encoding an enhanced green fluorescence protein (EGFP) using BMDCs *in vitro*. First, we compared the mRNA transfection efficiency of sugar-capsules coated with either one, two, or three layers of PEI-mRNA. Interestingly, sugar-capsules with a single layer of PEI-mRNA outperformed others with two or

https://dx.doi.org/10.1021/acs.nanolett.9b03483
Nano Lett. 2020, 20, 1499–1509

three layers of PEI-mRNA ($P < 0.0001$, Figure 3e,f), presumably due to more compact LbL structures for double- and triple-layered structures that require more time for intracellular unpacking and processing of mRNA. Based on these results, we performed all of the subsequent studies with single-layered sugar-capsules. Microplate-based quantification revealed robust translation of mEGFP by Mann-capsules, with a 4.9-fold and 4.6-fold higher EGFP signal by day 2, compared with PEI and lipofectamine, respectively ($P < 0.0001$, Figure 3g and Supporting Figure S12). Dex-capsules also induced robust expression of EGFP, as shown by the 10-fold and 9.3-fold improvement in EGFP signal by day 2, compared with PEI and lipofectamine, respectively ($P < 0.0001$, Figure 3g and Supporting Figure S12). Mann- and Dex-capsules did not affect the viability of BMDCs in all doses tested in our studies, whereas PEI and lipofectamine induced significant dose-dependent cytotoxicity (Figure 3h). Confocal microscopy revealed that, within 12 h of incubation, BMDCs cultured with mEGFP-Mann-capsules exhibited a prominent EGFP signal colocalized with Mann-Cy5.5-capsules signal in the cytoplasm, indicating translation of mRNA near Mann-capsules (Figure 3i). These results demonstrate that sugar-capsules are a biocompatible and effective delivery platform for mRNA.

Cancer vaccines aim to amplify CTL responses by promoting antigen presentation via MHC-I molecules on APCs (signal 1) and inducing costimulatory signals (signal 2) for cross-priming of CD8α+ T-cells (Figure 4a). We investigated whether mRNA delivered by sugar-capsules can promote antigen translation and presentation by DCs. We incubated BMDCs with mOVA-sugar-capsules and measured antigen presentation using 25-D1.16 monoclonal antibody that recognizes the complex between H-2K^b and SIINFEKL, a MHC-I minimal epitope derived from OVA. Incubation of BMDCs with mOVA-Mann-capsules significantly improved SIINFEKL-H-2K^b presentation by 12-fold and 5.8-fold, compared with PEI or lipofectamine, respectively ($P < 0.0001$, Figure 4b,c). Notably, Mann-capsules improved antigen presentation by 1.8-fold, compared with Dex-capsules ($P < 0.0001$, Figure 4b,c), potentially due to the differential engagement of PRRs by Mann- and Dex-capsules (Figure 3d).

We next examined cross-priming of antigen-specific CD8α+ T-cells using carboxyfluorescein succinimidyl ester (CFSE) dilution assay with SIINFEKL-specific CD8α+ T-cells from OT-I transgenic mice (OT-I T-cells).[37] BMDCs treated with mOVA delivered via Mann- or Dex-capsules significantly enhanced CFSE dilution and proliferation of OT-I T-cells, compared with mOVA, OVA protein + CpG, or blank sugar-capsules ($P < 0.0001$, Figure 4d–f). These results demonstrate that sugar-capsules are efficient mRNA delivery platforms for achieving robust antigen-specific T-cell responses.

Lastly, we evaluated the therapeutic efficacy of mRNA-sugar-capsules in a murine model of B16F10-OVA melanoma. Mice were inoculated s.c. with B16F10-OVA cells on day 0, and when the tumors were palpable on day 5, animals were vaccinated s.c. at the tail base with PBS, mOVA, mOVA-Dex-capsules, or mOVA-Mann-capsules (Figure 5a). The animals received boost immunizations on days 10 and 15. Mice treated with mOVA-Mann-capsule exhibited significantly delayed tumor growth, compared with PBS and mOVA ($P < 0.0001$, Figure 5b). On the other hand, treatment with mOVA-Dex-capsules led to an only modest reduction in tumor growth. Compared with tumor-bearing mice treated with mOVA, mice treated with mOVA-Mann-capsules had 4.5-fold and 4.1-fold higher numbers of splenic IFN-γ+ CD8α+ T-cells specific to $OVA_{257-264}$ (OVA-I, an immunodominant CD8α+ T-cell epitope) and IFN-γ+ CD4+ T-cells specific to $OVA_{323-339}$ (OVA-II, an immunodominant CD4 T-cell epitope), respectively ($P < 0.01$, Figure 5c,d). Notably, compared to mOVA-Dex-capsules, vaccination with mOVA-Mann-capsules achieved 4.3-fold and 10.8-fold higher numbers of antigen-specific IFN-γ+ CD8α+ and CD4+ T-cells, respectively ($P < 0.01$, Figure 5c,d). Importantly, vaccination with mOVA-Mann-capsules markedly enhanced tumor infiltration of CD8α+ T-cells (Figure 5e, Supporting Figure S13), with 130-fold and 11-fold higher frequency of tetramer+CD8α+ T-cells, compared with the mOVA and mOVA-Dex-capsules groups, respectively ($P < 0.0001$, Figure 5f,g). Also, mOVA-Mann-capsules treatment significantly improved the intratumoral infiltration of CD4+ T-cells, compared with mOVA and mOVA-Dex-capsules ($P < 0.05$ and $P < 0.01$, respectively, Figure 5h, Supporting Figure S14). Furthermore, mOVA-Mann-capsules treatment increased the activation of intratumoral DCs and tumor infiltration of NK cells, compared with mOVA-Dex-capsules ($P < 0.05$, Figure 5i,j). These *in vivo* studies show strong innate and adaptive immune responses with antitumor efficacy supported by Mann-capsule vaccination.

Interestingly, whereas Dex-capsules exhibited a high efficiency of mEGFP translation *in vitro* (Figure 3e), we observed that Mann-capsules promoted stronger antigen presentation *in vitro* (Figure 4b), more efficient trafficking to DCs in draining LNs (Figure 2g,f), and more potent elicitation of antigen-specific CD8α+ and CD4+ T-cells with antitumor efficacy *in vivo* (Figure 5). While this is beyond the scope of this initial report, we speculate that the specific interactions between Mann-capsules and PPRs in DCs may promote antigen processing and presentation, and we are currently working to delineate the molecular pathways for Mann-capsule-induced immune activation.

In summary, we have demonstrated for the first time that microbe-inspired sugar-capsules serve as a potent delivery platform for mRNA vaccines. By exploiting PAMP–PRR interactions, these sugar-capsules allow for strong activation of innate and adaptive immune responses. In particular, Mann-capsules trigger robust antitumor immune responses and may be utilized as a component in combination cancer immunotherapy with immune checkpoint blockade,[4] which will be the subject of our future studies. Our unique strategy of exploiting microbial components for constructing immunostimulatory materials may be generally applicable for the development of biomaterial-based vaccines and immunotherapies.

EXPERIMENTAL SECTION

Reagents and Instruments. Carboxyl-functionalized silica nanoparticles (~237 nm in diameter) were purchased from microparticles GmbH (Volmerstraße 9, 12489 Berlin, Germany). Sodium meta-periodate and dimethyl 3,3′-dithiobispropionimidate·2HCl (DTBP) were obtained from Thermofisher Scientific (Rockford, IL, USA). Mannan from *Saccharomyces cerevisiae*, triethylamine (TEA), ammonium fluoride, and polyethylenimine (PEI) (branched, MW 25,000) were obtained from Sigma-Aldrich (St. Louis, MO, USA). Dextran (MW ~ 40,000) was obtained from TCI AMERICA (Portland, OR, USA). mRNA encoding EGFP and OVA protein were from Trilink (San Diego, CA, USA). UV–

https://dx.doi.org/10.1021/acs.nanolett.9b03483
Nano Lett. 2020, 20, 1499–1509

vis absorption and fluorescence were measured using a BioTek synergy neo microplate reader. Transmission electron microscope (TEM) images were acquired using a JEOL 1400-plus instrument, and an atomic force microscope (AFM) was performed using Asylum-1 MFP-3D. Hydrodynamic size and zeta potential were measured using NanoSight NS300 and Malvern Zetasizer Nano ZSP instruments. Flow cytometry analyses were performed using a Ze5 instrument (Beckman Coulter, USA), and the data were analyzed using FlowJo 10.2 software. The mRNA loading amount was analyzed using gel permeation chromatography (GPC, Shimadzu). Confocal microscopy images were taken with a Leica SP8 confocal microscope. Mannan is from *Saccharomyces cerevisiae*.

Oxidation of Polysaccharide (Polysaccharide-CHO). Dextran (Dex) or mannan (Mann) was oxidized to generate aldehyde functional groups for further chemical modification. A 0.2 mg portion of polysaccharide was dissolved in 5 mL of ultrapure water, mixed with 5 mL of 0.01 M sodium periodate solution, and incubated for 1 h with gentle shaking at room temperature in the dark. The reactants were purified using a dialysis membrane (MWCO = 3000 Da, Spectrum) against deionized water for 3 days and lyophilized by freeze-drying in the dark for 2−3 days. The aldehyde content of polysaccharide-CHO was quantified using a modified hydroxylamine hydrochloride method.[38] The resulting polysaccharide-CHO was stored at 4 °C in the dark until further use.

Synthesis and Characterization of Polysaccharide-Based Nanocapsules. Carboxylated silica nanoparticles (siNPs) (~200 nm in diameter) were used as a template to construct a hollow polysaccharide nanocapsule. A 150 μL portion of aqueous PEI25K solution (10 mg/mL in ultrapure water) was added to 15 mg of carboxylated siNP in ultrapure water (900 μL), followed by vigorous vortexing for 10 min to introduce a positive charge on the surface of carboxylated siNP (PEI-siNP). PEI-siNP was purified three times using ultracentrifugation for 2 min at 18,500 rpm. PEI-siNP was then chemically cross-linked with dimethyl 3,3′-dithiobispropionimidate·2HCl (DTBP) cross-linker (0.5 mg in 1 mL of 0.1 M TEA buffer at pH 8) for 1 h at room temperature, followed by three rounds of purifications with ultrapure water. The PEI content was analyzed using 2,4,6-trinitrobenzenesulfonic acid (TNBSA, ThermoFisher) solution by quantifying primary amine groups per PEI. For mRNA loading, mRNA (100 μL, 500 μg/mL) was added to cross-linked-PEI-siNP solution (900 μL, 15 mg), incubated for 10 min with vigorous vortexing, and purified twice with ultrapure water. Loading of mRNA was analyzed by agarose gel electrophoresis (15%, 100 V, 20 min) and GPC equipped with a TSKgel G3000SWxl column (7.8 mm ID X 300 mm, Tosoh Bioscience LLC). Polysaccharide-CHO (1000 μL, 2 mg/mL) was chemically introduced into the outermost surface of PEI-siNPs in ultrapure water for 12 h at room temperature by amine−aldehyde reaction between PEI and polysaccharide-CHO (polysaccharide-siNP). The siNP core of polysaccharide-siNP was removed by ammonium fluoride for 5 min at room temperature and washed three times with ultrapure water, followed by PBS twice to produce hollow sugar-capsules. For physicochemical characterizations of sugar-capsules, TEM and AFM were performed. Sugar-capsules were stored at 4 °C until further use. The endotoxin level for each *in vivo* dose of sugar-capsule and polysaccharide was measured to be less than 0.05 EU/mg/dose, as determined by the LAL Chromogenic Endotoxin Quantitation Kit (Pierce).

DLS and Extrusion. The hydrodynamic size and zeta potential of nanoparticles were measured using a Malvern Zetasizer Nano ZS after diluting samples in deionized water. Extrusion was performed by passing samples through a filter membrane of 200, 100, or 50 nm pore size using a Mini Extruder (Avanti polar lipid). After 13 times of extrusion to the alternating syringes at room temperature, the recovery of samples was quantified by UV−vis spectrometry.

Serum Stability of Cy5.5 Conjugates. Mann-Cy5.5 or Mann-Cy5.5-capsule were diluted in PBS supplemented with 10% FBS or 50% FBS and incubated at 37 °C in the dark. Release of Cy5.5 was quantified at the indicated time points by separating free Cy5.5 using Amicon ultra centrifugal filters with a Mw cutoff of 3 kDa (MilliporeSigma), followed by fluorescence measurement.

BMDC Uptake, Cytotoxicity, and mRNA Transfection. Bone-marrow-derived dendritic cells (BMDCs) were prepared according to the literature.[39] Briefly, cells were aseptically isolated from femurs and tibia of C57BL/6 mice and cultured in complete DC media comprised of RPMI-1640 (Gibco) supplemented with 10% fetal bovine serum (FBS, Corning), 1% penicillin/streptomycin (Gibco), 55 μM β-mercaptoethanol (Gibco), and 20 ng/mL granulocyte−macrophage colony-stimulating factor (GM-CSF, Genscript) at 37 °C with 5% CO_2. Fresh media was added on day 3, and all media was renewed on days 6 and 8. The cultured BMDCs were used between days 7 and 12. For NP dose- and time-dependent uptake study, immature BMDCs in complete DC media were plated and cultured overnight at 105 cells per well in a 96-well plate and treated with the varying concentrations of formulations for the indicated duration. BMDCs were then harvested with cell dissociation reagent (StemPro Accutase, Gibco) and washed twice with cold PBS. BMDCs were incubated with anti-CD16/32 Fcγ blocking antibody (eBioscience) for 10 min and stained with anti-CD11c antibody (Biolegend) for 30 min at room temperature. The cells were washed twice with FACS buffer (1% BSA in PBS) and dispersed in FACS buffer with DAPI (300 nM) for flow cytometry analysis. For cytotoxicity study, after 24 h incubation with NPs, viable BMDCs were quantified by cell counting kit (CCK)-8 (Dojindo Molecular Technologies) according to the manufacturer's instructions. For mRNA transfection study, 5-methoxyuridine modified mRNA encoding EGFP (EGFP-mRNA) was loaded into sugar-capsules as well as Lipofectamine 2000 (ThermoFisher Scientific) and BPEI as control groups. All other procedures are the same as the uptake study. For intracellular visualization of mRNA translation using a confocal microscope, 5×10^5 BMDCs seeded on the coverslip-bottom 12-well plate were treated with Cy5.5-labeled sugar-capsules loaded with EGFP-mRNA for 12 h. BMDCs were washed three times with cold PBS, stained with DAPI in PBS (300 nM), and fixed with 4% formaldehyde for 30 min. After mounting coverslips with a mounting media (Vector Laboratories), cells were imaged by a confocal microscope.

Incubation with HEK-Blue TLR Cells. HEK-blue TLR4 and TLR9 cells were obtained from Invivogen and maintained according to the manufacturer's instruction. Cells were incubated with 25 μg/mL samples in HEK-Blue Detection medium. LPS (1 μg/mL) and CpG (10 μg/mL) were employed as positive controls TLR4 and TLR9, respectively. The activation of TLR cells was quantified after 8 h by absorbance reading at 650 nm with correction of the sample

https://dx.doi.org/10.1021/acs.nanolett.9b03483
Nano Lett. 2020, 20, 1499−1509

effect by subtracting the absorbance of samples without TLR cells.

BMDC Activation and Antigen Presentation and Cross-Priming. BMDCs in complete DC media were plated at 10^5 cells per well in a 96-well plate. After overnight incubation, BMDCs were treated with various NP formulations or control groups, including soluble OVA-mRNA (1 μg/well) and CpG (1 μM, Integrated DNA technologies). Supernatants were collected and analyzed for cytokines, including IL-12p70, TNF-α, and IL-6. BMDCs were then harvested and incubated with anti-CD16/32 blocking antibody at room temperature for 10 min, and stained at room temperature for 30 min with fluorophore-labeled antibodies against CD11c (Biolegend), CD40 (e-bioscience), CD86 (eBioscience), and MHCII (Biolegend) or antimouse SIINFEKL/H-2Kb monoclonal antibody 25-D1.16 (eBioscience) for antigen presentation. Cells were analyzed by flow cytometry analysis.

T-Cell Expansion. To assess cross-priming of T-cells by OVA-mRNA loaded sugar-capsule (mOVA-sugar-capsule), 10^5 BMDCs in 96-well plates were pulsed with mOVA-sugar-capsule or control groups, including OVA protein (250 μg/mL)/CpG (5 μg/mL) and soluble mOVA (5 μg/mL) for 4 or 24 h. BMDCs were washed three times with PBS to remove free NPs. Spleens were harvested from OT-I and OT-II transgenic mice, and CD8α+ and CD4+ T-cells were isolated using a negative selection kit (Stemcell Technology), respectively. After labeling them with carboxyfluorescein succinimidyl ester (CFSE, 0.1 μM, 2×10^6 cells/mL, 10 min in RPMI), T-cells were washed and transferred to the BMDC-containing 96-wells. After 3 days of coculture, T-cells were harvested and stained with anti-CD8α (eBioscience) for flow cytometry analysis.

Pattern Recognition Receptor Inhibition Study with Blocking Antibodies (ELISA and Multiplex). 2×10^5 BMDCs in complete DC media were seeded on a 24-well plate overnight. Each PRR receptor on the BMDC surface was blocked by the corresponding blocking antibody for 30 min at a final concentration of 2 μg/mL against Dectin-1, Dectin-2, CD206, CD209 (DC-SIGN), Mincle, TLR-2, and TLR-4 receptors, followed by NP treatment. All PRR blocking antibodies were from Invivogen. A phagocytosis inhibitor, Latrunculin (Invitrogen), was also included for some groups. After 24 h of incubation, supernatants were collected for cytokine analysis by ELISA (R&D system) or Luminex multiflex assays (Luminex MAGPIX).

Lymphatic Draining Efficacy. C57BL/6 mice were subcutaneously administered at the tail base with native-Mann, silica-Mann, and Mann-capsule. The Cy5.5 fluorescence intensity of the three formulations was quantified and normalized before injection using a microplate reader with Ex = 650 and Em = 665 nm. Inguinal LNs were harvested and imaged using IVIS to quantify Cy5.5 fluorescence signals. LNs were homogenized by pestle motor (Argos Technologies) and treated with collagenase type IV (1 mg/mL) and DNase I (100 U/mL) at 37 °C for 30 min with gentle shaking to prepare single-cell suspensions. LN cells were filtered through a 40 μm cell strainer, washed twice, and stained by fluorophore-labeled antibodies for flow cytometry analysis. DCs were identified by antibodies against MHC-II (Biolegend) and CD11c (Biolegend), and their activation was examined using antibodies against CD80 (BD Biosciences) and CD86 (BD Biosciences).

Animal Experiments. Animals were cared for following the federal, state, and local guidelines. All work performed on animals was in accordance with and approved by the Institutional Animal Care and Use Committee (IACUC) at the University of Michigan, Ann Arbor. Female C57BL/6 (5−6 weeks) were purchased from Envigo (USA). For the mRNA vaccination study, C57BL/6 mice were subcutaneously injected with 2×10^5 B16F10-OVA cells per mouse at the right flank on day 0 and immunized on days 7, 12, and 17 with mOVA (10 μg), mOVA-Dex-capsule (10 μg mRNA, 1000 μg Dex-capsule in 100 μL of PBS), and mOVA-Mann-capsule (10 μg mOVA, 1000 μg Mann-capsule in 100 μL of PBS). Tumor growth was measured two to three times a week, and the tumor volume was calculated by the ellipsoidal calculation as $V = (\text{width})^2 \times \text{length} \times 0.52$. Animals were euthanized when individual tumor masses reached 1.5 cm in diameter or when animals became moribund.

Tetramer Staining and ELISPOT. For analysis of tumor-antigen-specific CD8α+ T-cells in the systemic circulation, submandibular bleeding was performed at indicated time points. Red blood cells in PBMCs were lysed with ACK lysis buffer twice at room temperature, followed by two washing steps with FACS buffer. PBMCs were blocked with CD16/32 antibody for 10 min and then stained with H-2K^b OVA tetramer-SINNFEKL (MBL International) and anti-CD8α (BD Biosciences) for flow cytometry analysis. ELISPOT assay was performed with splenocytes from immunized mice. Splenocytes were harvested aseptically, processed into a single-cell suspension, and plated with 5×10^5 splenocytes per well in 96-well PVDF plates (EMD Millipore) precoated with IFN-γ antibody (R&D Systems) overnight. Splenocytes were then restimulated with antigen peptides (2 μg/mL) or controls for 24 h. Assays were completed using sequential incubations with biotinylated-secondary antibody, streptavidin alkaline phosphatase (Sigma Chemical), and NBT/BCIP substrate (Surmodics). Developed spots were analyzed using an AID iSpot Reader (Autoimmun Diagnostika GmbH, Germany).

Tumor Microenvironment Analysis. Tumors excised on day 26 after injection were homogenized using pestle motor and treated with collagenase type IV (1 mg/mL) and DNase I (100 U/mL) in serum-free RPMI for 30 min at 37 °C with gentle shaking. The cell suspension was passed through a cell strainer (70 μm) and washed with FACS buffer twice. Cells were then incubated with CD16/32 blocking antibody at 1:20 dilution for 10 min and then stained with antibodies for 30 min at room temperature against CD8, CD4, and NK cells. For the staining of CD8 T-cells, CD45-FITC (eBiosciene), H-2K^b OVA tetramer-SIINFEKL-PE (MBL International), CD8α-APC (BD Bioscience), and CD3-PE-CY7 (Biolegend) were used. For CD4 T-cells, CD45-FITC (eBiosciene), CD4-APC (eBioscience), CD3-PE-CY7 (Biolegend) were used, and for DCs, CD45-FITC (eBiosciene), CD11c-PE (Biolegend), and CD86-PE-CY7 (BD Bioscience) were used. For NK cell staining, CD45-FITC (eBiosciene), NK1.1-PE (eBioscience), and CD3-PE-CY7 (Biolegend) were used. In all flow cytometric analyses, antibodies were used at 1:100 dilution, and only DAPI negative live cells were gated out and analyzed.

Immunofluorescence Staining. Tumors were collected, and frozen sections were prepared at 7 μm thickness by cryostat sectioning. After fixing in cooled acetone for 10 min and blocking with 10% goat serum, the sections were incubated with primary antibodies against CD4 (ThermoFisher #PA5-87425) and CD8 (ThermoFisher #14-0081-82) overnight at 4 °C, followed by incubation with AF488- and AF647-conjugated secondary antibodies for 1 h at room

https://dx.doi.org/10.1021/acs.nanolett.9b03483
Nano Lett. 2020, 20, 1499−1509

temperature (ThermoFisher #A32731 and #A21247 for CD4 and CD8, respectively). After staining with DAPI for another 10 min, the sections were mounted with coverslips using a prolong diamond mounting medium for observation under confocal microscopy (Nikon A1Rsi Confocal Microscope).

Statistical Analysis. For animal studies, mice were randomized to match the similar average volume of the primary tumors before the initiation of any treatments. All procedures were performed in a nonblinded fashion. Statistical analysis was performed with Prism 6.0 software (GraphPad Software) by one-way or two-way ANOVA with Bonferroni multiple comparisons post-test. The statistical significance for the survival curve was calculated by the log-rank test. Data were approximately normally distributed, and variance was similar between the groups. Statistical significance is indicated as $*P < 0.05$, $**P < 0.01$, $***P < 0.001$, and $****P < 0.0001$.

■ ASSOCIATED CONTENT

Supporting Information

The Supporting Information is available free of charge at https://pubs.acs.org/doi/10.1021/acs.nanolett.9b03483.

Figures related to the following: measurement of hydrodynamic size and surface charge, determination of mRNA loading after each LbL procedure, GPC analysis of mRNA recovered from Mann-capsules, colloidal stability of mRNA-sugar-capsules, quantification of mRNA loading, hydrodynamic size and surface charge of silica-NP, Mann-silica, and Mann-capsule, measurement of the stiffness of Mann-capsules, serum stability of Cy5.5 conjugated native-Mann and Mann-capsule, confocal images of BMDCs and BMDMs incubated with Mann- or Dex-capsules, BMDC uptake of Dex- and Mann-capsules, activation of TLR4 and TLR9 by Mann- and Dex-capsules, mRNA translation efficacy of mRNA-sugar-capsules, gating strategy for flow cytometric analysis of tumor tissues, and immunohistochemistry images of T-cells in tumors (PDF)

■ AUTHOR INFORMATION

Corresponding Authors

Omid C. Farokhzad − *Center for Nanomedicine and Department of Anesthesiology, Brigham and Women's Hospital, Harvard Medical School, Boston, Massachusetts 02115, United States;* orcid.org/0000-0003-2009-270X; Email: ofarokhzad@bwh.harvard.edu

James J. Moon − *Department of Pharmaceutical Sciences, Biointerfaces Institute, and Department of Biomedical Engineering, University of Michigan, Ann Arbor, Michigan 48109, United States;* orcid.org/0000-0003-2238-2372; Email: moonjj@umich.edu

Authors

Sejin Son − *Department of Pharmaceutical Sciences and Biointerfaces Institute, University of Michigan, Ann Arbor, Michigan 48109, United States; Center for Nanomedicine and Department of Anesthesiology, Brigham and Women's Hospital, Harvard Medical School, Boston, Massachusetts 02115, United States;* orcid.org/0000-0003-1523-2990

Jutaek Nam − *Department of Pharmaceutical Sciences and Biointerfaces Institute, University of Michigan, Ann Arbor, Michigan 48109, United States;* orcid.org/0000-0002-0397-1449

Ilia Zenkov − *Center for Nanomedicine and Department of Anesthesiology, Brigham and Women's Hospital, Harvard Medical School, Boston, Massachusetts 02115, United States*

Lukasz J. Ochyl − *Department of Pharmaceutical Sciences and Biointerfaces Institute, University of Michigan, Ann Arbor, Michigan 48109, United States*

Yao Xu − *Department of Pharmaceutical Sciences and Biointerfaces Institute, University of Michigan, Ann Arbor, Michigan 48109, United States*

Lindsay Scheetz − *Department of Pharmaceutical Sciences and Biointerfaces Institute, University of Michigan, Ann Arbor, Michigan 48109, United States*

Jinjun Shi − *Center for Nanomedicine and Department of Anesthesiology, Brigham and Women's Hospital, Harvard Medical School, Boston, Massachusetts 02115, United States;* orcid.org/0000-0001-9200-5068

Complete contact information is available at: https://pubs.acs.org/10.1021/acs.nanolett.9b03483

Author Contributions

S.S. and J.N. contributed equally to this work. S.S., O.C.F., and J.J.M. designed the study. S.S., J.N., I.Z., L.J.O., Y.X., and L.S. performed the experiments. S.S., J.N., J.S., and J.J.M. interpreted the data. S.S., J.N., O.C.F., and J.J.M. wrote the paper.

Funding

This work was supported in part by NIH (R01EB022563, R01AI127070, R01CA210273, R01CA223804 and U01CA210152), MTRAC for Life Sciences Hub, and Emerald Foundation) and David Koch-Prostate Cancer Foundation Award in Nanotherapeutics. J.J.M. is a Young Investigator supported by the Melanoma Research Alliance (348774), DoD/CDMRP Peer Reviewed Cancer Research Program (W81XWH-16-1-0369), and NSF CAREER Award (1553831). Opinions, interpretations, conclusions, and recommendations are those of the authors and are not necessarily endorsed by the Department of Defense.

Notes

The authors declare the following competing financial interest(s): O.C.F. has financial interest in Selecta Biosciences, Tarveda Therapeutics, and Seer.

■ ACKNOWLEDGMENTS

We acknowledge the NIH Tetramer Core Facility (contract HHSN272201300006C) for provision of MHC-I tetramers.

■ REFERENCES

(1) Banchereau, J.; Steinman, R. M. Dendritic cells and the control of immunity. *Nature* **1998**, *392* (6673), 245−52.

(2) Mogensen, T. H. Pathogen recognition and inflammatory signaling in innate immune defenses. *Clin. Microbiol. Rev.* **2009**, *22* (2), 240−73.

(3) Ozinsky, A.; Underhill, D. M.; Fontenot, J. D.; Hajjar, A. M.; Smith, K. D.; Wilson, C. B.; Schroeder, L.; Aderem, A. The repertoire for pattern recognition of pathogens by the innate immune system is defined by cooperation between toll-like receptors. *Proc. Natl. Acad. Sci. U. S. A.* **2000**, *97* (25), 13766−71.

(4) Nam, J.; Son, S.; Park, K. S.; Zou, W.; Shea, L. D.; Moon, J. J. Cancer nanomedicine for combination cancer immunotherapy. *Nature Reviews Materials* **2019**, *4* (6), 398−414.

(5) Han, X.; Shen, S.; Fan, Q.; Chen, G.; Archibong, E.; Dotti, G.; Liu, Z.; Gu, Z.; Wang, C. Red blood cell-derived nanoerythrosome for

antigen delivery with enhanced cancer immunotherapy. *Sci. Adv.* **2019**, *5* (10), No. eaaw6870.
(6) Pardi, N.; Hogan, M. J.; Porter, F. W.; Weissman, D. mRNA vaccines - a new era in vaccinology. *Nat. Rev. Drug Discovery* **2018**, *17* (4), 261−279.
(7) Hajj, K. A.; Whitehead, K. A. Tools for translation: non-viral materials for therapeutic mRNA delivery. *Nature Reviews Materials* **2017**, *2*, 17056.
(8) Stanton, M. G. Current Status of Messenger RNA Delivery Systems. *Nucleic Acid Ther.* **2018**, *28* (3), 158−165.
(9) Kreiter, S.; Selmi, A.; Diken, M.; Koslowski, M.; Britten, C. M.; Huber, C.; Türeci, Ö.; Sahin, U. Intranodal Vaccination with Naked Antigen-Encoding RNA Elicits Potent Prophylactic and Therapeutic Antitumoral Immunity. *Cancer Res.* **2010**, *70* (22), 9031−9040.
(10) Weide, B.; Pascolo, S.; Scheel, B.; Derhovanessian, E.; Pflugfelder, A.; Eigentler, T. K.; Pawelec, G.; Hoerr, I.; Rammensee, H. G.; Garbe, C. Direct injection of protamine-protected mRNA: results of a phase 1/2 vaccination trial in metastatic melanoma patients. *J. Immunother.* **2009**, *32* (5), 498−507.
(11) Fotin-Mleczek, M.; Duchardt, K. M.; Lorenz, C.; Pfeiffer, R.; Ojkic-Zrna, S.; Probst, J.; Kallen, K. J. Messenger RNA-based vaccines with dual activity induce balanced TLR-7 dependent adaptive immune responses and provide antitumor activity. *J. Immunother.* **2011**, *34* (1), 1−15.
(12) Perche, F.; Benvegnu, T.; Berchel, M.; Lebegue, L.; Pichon, C.; Jaffres, P. A.; Midoux, P. Enhancement of dendritic cells transfection in vivo and of vaccination against B16F10 melanoma with mannosylated histidylated lipopolyplexes loaded with tumor antigen messenger RNA. *Nanomedicine* **2011**, *7* (4), 445−53.
(13) Oberli, M. A.; Reichmuth, A. M.; Dorkin, J. R.; Mitchell, M. J.; Fenton, O. S.; Jaklenec, A.; Anderson, D. G.; Langer, R.; Blankschtein, D. Lipid Nanoparticle Assisted mRNA Delivery for Potent Cancer Immunotherapy. *Nano Lett.* **2017**, *17* (3), 1326−1335.
(14) Uchida, S.; Kinoh, H.; Ishii, T.; Matsui, A.; Tockary, T. A.; Takeda, K. M.; Uchida, H.; Osada, K.; Itaka, K.; Kataoka, K. Systemic delivery of messenger RNA for the treatment of pancreatic cancer using polyplex nanomicelles with a cholesterol moiety. *Biomaterials* **2016**, *82*, 221−8.
(15) Islam, M. A.; Xu, Y.; Tao, W.; Ubellacker, J. M.; Lim, M.; Aum, D.; Lee, G. Y.; Zhou, K.; Zope, H.; Yu, M.; Cao, W.; Oswald, J. T.; Dinarvand, M.; Mahmoudi, M.; Langer, R.; Kantoff, P. W.; Farokhzad, O. C.; Zetter, B. R.; Shi, J. Restoration of tumour-growth suppression in vivo via systemic nanoparticle-mediated delivery of PTEN mRNA. *Nature Biomedical Engineering* **2018**, *2* (11), 850−864.
(16) Lin, K.; Kasko, A. M. Carbohydrate-Based Polymers for Immune Modulation. *ACS Macro Lett.* **2014**, *3* (7), 652−657.
(17) Tzianabos, A. O. Polysaccharide immunomodulators as therapeutic agents: structural aspects and biologic function. *Clin. Microbiol. Rev.* **2000**, *13* (4), 523−33.
(18) Ghotbi, Z.; Haddadi, A.; Hamdy, S.; Hung, R. W.; Samuel, J.; Lavasanifar, A. Active targeting of dendritic cells with mannan-decorated PLGA nanoparticles. *J. Drug Targeting* **2011**, *19* (4), 281−92.
(19) Hamdy, S.; Haddadi, A.; Shayeganpour, A.; Samuel, J.; Lavasanifar, A. Activation of antigen-specific T cell-responses by mannan-decorated PLGA nanoparticles. *Pharm. Res.* **2011**, *28* (9), 2288−301.
(20) Haddadi, A.; Hamdy, S.; Ghotbi, Z.; Samuel, J.; Lavasanifar, A. Immunoadjuvant activity of the nanoparticles' surface modified with mannan. *Nanotechnology* **2014**, *25* (35), 355101.
(21) Vetvicka, V. Glucan-immunostimulant, adjuvant, potential drug. *World journal of clinical oncology* **2011**, *2* (2), 115−9.
(22) Feng, Y.; Mu, R.; Wang, Z.; Xing, P.; Zhang, J.; Dong, L.; Wang, C. A toll-like receptor agonist mimicking microbial signal to generate tumor-suppressive macrophages. *Nat. Commun.* **2019**, *10* (1), 2272.
(23) Sun, B.; Yu, S.; Zhao, D.; Guo, S.; Wang, X.; Zhao, K. Polysaccharides as vaccine adjuvants. *Vaccine* **2018**, *36* (35), 5226−5234.
(24) Romani, L. Immunity to fungal infections. *Nat. Rev. Immunol.* **2011**, *11* (4), 275−88.
(25) Schenten, D.; Medzhitov, R. The control of adaptive immune responses by the innate immune system. *Adv. Immunol.* **2011**, *109*, 87−124.
(26) Pustylnikov, S.; Sagar, D.; Jain, P.; Khan, Z. K. Targeting the C-type lectins-mediated host-pathogen interactions with dextran. *J. Pharm. Pharm. Sci.* **2014**, *17* (3), 371−92.
(27) Hawley, A. E.; Davis, S. S.; Illum, L. Targeting of colloids to lymph nodes: influence of lymphatic physiology and colloidal characteristics. *Adv. Drug Delivery Rev.* **1995**, *17* (1), 129−148.
(28) Siram, K.; Chellan, V. R.; Natarajan, T.; Krishnamoorthy, B.; Mohamed Ebrahim, H. R.; Karanam, V.; Muthuswamy, S. S.; Ranganathan, H. P. Solid lipid nanoparticles of diethylcarbamazine citrate for enhanced delivery to the lymphatics: in vitro and in vivo evaluation. *Expert Opin. Drug Delivery* **2014**, *11* (9), 1351−65.
(29) Ali, M.; Afzal, M.; Bhattacharya, S. M.; Ahmad, F. J.; Dinda, A. K. Nanopharmaceuticals to target antifilarials: a comprehensive review. *Expert Opin. Drug Delivery* **2013**, *10* (5), 665−78.
(30) Li, S. D.; Huang, L. Pharmacokinetics and biodistribution of nanoparticles. *Mol. Pharmaceutics* **2008**, *5* (4), 496−504.
(31) Kaminskas, L. M.; Kota, J.; McLeod, V. M.; Kelly, B. D.; Karellas, P.; Porter, C. J. PEGylation of polylysine dendrimers improves absorption and lymphatic targeting following SC administration in rats. *J. Controlled Release* **2009**, *140* (2), 108−16.
(32) Rao, D. A.; Forrest, M. L.; Alani, A. W.; Kwon, G. S.; Robinson, J. R. Biodegradable PLGA based nanoparticles for sustained regional lymphatic drug delivery. *J. Pharm. Sci.* **2010**, *99* (4), 2018−31.
(33) Feng, L.; Zhang, L.; Liu, M.; Yan, Z.; Wang, C.; Gu, B.; Liu, Y.; Wei, G.; Zhong, G.; Lu, W. Roles of dextrans on improving lymphatic drainage for liposomal drug delivery system. *J. Drug Targeting* **2010**, *18* (3), 168−78.
(34) Mueller, S. N.; Tian, S.; DeSimone, J. M. Rapid and Persistent Delivery of Antigen by Lymph Node Targeting PRINT Nanoparticle Vaccine Carrier To Promote Humoral Immunity. *Mol. Pharmaceutics* **2015**, *12* (5), 1356−65.
(35) Nam, J.; Son, S.; Moon, J. J. Adjuvant-Loaded Spiky Gold Nanoparticles for Activation of Innate Immune Cells. *Cell. Mol. Bioeng.* **2017**, *10* (5), 341−355.
(36) Son, S.; Singha, K.; Kim, W. J. Bioreducible BPEI-SS-PEG-cNGR polymer as a tumor targeted nonviral gene carrier. *Biomaterials* **2010**, *31* (24), 6344−54.
(37) Quah, B. J.; Warren, H. S.; Parish, C. R. Monitoring lymphocyte proliferation in vitro and in vivo with the intracellular fluorescent dye carboxyfluorescein diacetate succinimidyl ester. *Nat. Protoc.* **2007**, *2* (9), 2049−56.
(38) Zhao, H.; Heindel, N. D. Determination of Degree of Substitution of Formyl Groups in Polyaldehyde Dextran by the Hydroxylamine Hydrochloride Method. *Pharm. Res.* **1991**, *8* (3), 400−402.
(39) Lutz, M. B.; Kukutsch, N.; Ogilvie, A. L.; Rossner, S.; Koch, F.; Romani, N.; Schuler, G. An advanced culture method for generating large quantities of highly pure dendritic cells from mouse bone marrow. *J. Immunol. Methods* **1999**, *223* (1), 77−92.

https://dx.doi.org/10.1021/acs.nanolett.9b03483
Nano Lett. 2020, 20, 1499−1509